



Risk Comparison of Hurricane Scenarios as Disruptions of Hydrologic Basin Order with Social Vulnerability Criteria

Gigi Pavur, S.M.ASCE¹; James H. Lambert, F.ASCE²; and Venkataraman Lakshmi, F.ASCE³

Abstract: Economic damages of hurricanes and tropical cyclones are increasing faster than the populations and wealth of many coastal areas. There is urgency to update priorities of agencies engaged with risk assessment, risk mitigation, and risk communication across hundreds or thousands of water basins. This paper evaluates hydrology and social vulnerability factors to develop a risk register at a subbasin scale for which the priorities of agencies vary by storm scenario using publicly available satellite-based Earth observations. The novelty and innovation of this approach is the quantification and mapping of risk as a disruption of system order, while using social vulnerability indices and sensor data from disparate sources. The results assist with allocating resources across basins under several scenarios of hydrology and social vulnerability. The approach is in several parts as follows: first, a baseline order of basins is defined using the CDC/ATSDR social vulnerability index (SVI). Next, a set of storm scenarios is defined using Earth Observations and modeled data. Next, a swing-weight technique is used to update factor weights under each scenario. Lastly, the importance order of basins relative to the baseline order is used to compare the risk of scenarios across the study area. The risk is thus quantified (by least squares difference of order) as a disruption to the ordering of basins by social and hydrologic factors (i.e., SVI, precipitation, wind speed, and soil moisture), with attention to the most disruptive scenarios. An application is described with extensive mapping of hydrologic basins for Hurricane Ian to demonstrate a versatile method to address uncertainty of scenarios of storm nature and extent across coastal mega-regions. DOI: 10.1061/AJRUA6.RUENG-1228. This work is made available under the terms of the Creative Commons Attribution 4.0 International license, https://creativecommons.org/ licenses/by/4.0/.

Author keywords: Risk analysis; System analysis; Satellite data; Resource allocation; Scenario-based preferences.

Introduction

Tropical cyclones historically result in social, economic, and environmental losses in coastal mega-regions such as the southeastern United States. Compared to other disasters in the US, tropical cyclones result in the most damages and fatalities, averaging approximately \$30.9 billion in damages and 157 fatalities per year since 1980 (NOAA 2023). The southeastern US is a hotspot for disproportionately high losses from climate-sensitive hazards because of elevated exposure and concentrations of socially vulnerable populations (Cutter et al. 2003; Emrich and Cutter 2011). With predictions that climate change will increase the frequency and intensity of future tropical cyclones, there is a need to reduce tropical cyclone risk and improve system resilience (Lavell et al. 2012; UNDRR 2015). Evidence-based decision making has been identified as an essential tool to support sustainable, resilient, and risk-informed societies across organizational boundaries during

¹Graduate Research Fellow, Dept. of Civil and Environmental Engineering, Univ. of Virginia, Olsson Hall, P.O. Box 400747, Charlottesville, VA 22904-4747 (corresponding author). ORCID: https://orcid.org/0000 -0002-2473-8670. Email: gp3vd@virginia.edu

²Professor and Director, Center for Risk Management of Engineering Systems, Dept. of Systems and Information Engineering, Univ. of Virginia, Olsson Hall, P.O. Box 400747, Charlottesville, VA 22904-4747.

³Professor, Dept. of Civil and Environmental Engineering, Univ. of Virginia, Olsson Hall, P.O. Box 400747, Charlottesville, VA 22904-4747.

Note. This manuscript was submitted on September 4, 2023; approved on March 22, 2024; published online on July 15, 2024. Discussion period open until December 15, 2024; separate discussions must be submitted for individual papers. This paper is part of the ASCE-ASME Journal of Risk and Uncertainty in Engineering Systems, Part A: Civil Engineering, ©ASCE, ISSN 2376-7642.

disasters (Kavvada et al. 2022; Shittu et al. 2018). To support this, there is a need to quantify risk using social and environmental data.

The social vulnerability of an individual or community refers to their "capacity to anticipate, confront, repair, or recover from the effects of a disaster" (Flanagan et al. 2018). Previous studies have shown that communities of high social vulnerability face significant short- and long-term challenges following disasters, which limits their ability to recover (Flanagan et al. 2011, 2018; Fothergill and Peek 2004; Yarveysi et al. 2023). Disparities of social vulnerability are observable within neighboring blocks, meaning communities with varying social vulnerability will likely suffer different impacts if exposed to the same tropical cyclone conditions (Bakkensen et al. 2017; Yarveysi et al. 2023). For example, the overall economic cost of repairs may be larger within an affluent community, but the losses are disproportionately higher for the socially vulnerable community (Flanagan et al. 2011). Examples of tropical cyclone disaster challenges associated with social vulnerability during each phase of the disaster cycle (mitigation, preparedness, response, and recovery) are provided in the Appendix I.

Previous research quantified the relative social vulnerability of the United States at various spatial resolutions including the county level, Census-tract level, and block level (Cutter et al. 2003; Flanagan et al. 2011; Yarveysi et al. 2023). These data sets have been applied to natural and anthropogenic hazards to show the spatial and temporal variability of social vulnerability across the United States. Three social vulnerability indices are described below:

1. County-level social vulnerability index (SoVI): Cutter et al. (2003) developed the county-level SoVI by using principal components analysis with socioeconomic and demographic data that were identified as influential to natural hazards vulnerability (Cutter et al. 2003; Emrich and Cutter 2011). Findings included observable variations in SoVI across widespread regions, such as neighboring states, and the need for higher spatial resolution data to resolve hazard vulnerabilities at the subcounty level (Cutter et al. 2003; Emrich and Cutter 2011). Due to the coarse county-level resolution, SoVI was not used in this study.

- 2. Block-level socio-economic-infrastructure vulnerability index (SEIV): Yarveysi et al. (2023) developed the SEIV by leveraging machine learning algorithms to provide high-resolution vulnerability data at the block level (Yarveysi et al. 2023). This allows for analyses at finer spatial resolutions compared to SoVI and SVI. It showed significant inequities among neighboring blocks (Yarveysi et al. 2023). However, SEIV is not currently recommended to be applied to disasters with high levels of damage (>\$250 million) since losses at the fine resolution of SEIV are unreasonable to distinguish (Yarveysi et al. 2023). Since this study provides a demonstration of the methodology for a hurricane with damages of over \$114 billion, SEIV was not used.
- 3. Census-tract level social vulnerability index (SVI): The Centers for Disease Control (CDC) and Prevention Agency for Toxic Substances and Disease Register (ASTDR) constructed a Census-tract level SVI designed to support disaster management (Flanagan et al. 2011). The index is available for multiple years (2000, 2010, 2014, 2016, 2018, and 2020) using 16 variables to calculate SVI at national and state levels (see Appendix II; Flanagan et al. 2011). SVI has been validated and applied to natural and anthropogenic disasters including tropical cyclones, wildfires, sea level rise, rural/urban studies, migrant and refugee population studies, etc. (Flanagan et al. 2018). For this study, we have chosen to use SVI as it is the finest resolution social vulnerability data appropriate for disasters with extensive damage greater than \$250 million.

A factor of tropical cyclone damage is exposure to intense hydrometeorological conditions. Generally, adequate spatial and temporal ground-based in situ observations are not possible to collect during tropical cyclones due to widespread instrument failures (Bucci et al. 2022). Satellite-based Earth observations can fill this data gap by collecting high-resolution spatial and temporal data during the disaster, which may have otherwise been unobservable. For this study, precipitation, wind speed, and soil moisture estimates were obtained from Earth observations and models. Since hurricane damages can occur from exposure to a single extreme environmental variable as well as a combined exposure to multiple environmental variables, this study considers both individual and multiple variables (Clark et al. 2022).

With the above motivation, this paper will address a need for regularly updated disaster risk maps, as outlined in the United Nations Sendai Framework for Disaster Risk Reduction, by providing a methodology to combine disparate sources of information in a risk register at a subbasin scale (Bonato et al. 2022; Hamilton et al. 2015; Kaplan and Garrick 1981; Karvetski et al. 2009; UNDRR 2015; You et al. 2014). Within this risk register of basins, hydrological and social vulnerability factors (specifically SVI, cumulative precipitation, maximum hourly precipitation, maximum hourly wind speed, and 5-day antecedent soil moisture) are combined in several storm scenarios that disrupt the system order relative to a baseline scenario of SVI. A swing-weight technique is used to calculate new ordering functions for each basin under a given scenario (Karvetski et al. 2009). The swing-weight technique allows for tradeoffs of higher consideration of one or more variables in exchange for lower consideration of other variables (Karvetski et al. 2009). This is advantageous for risk analysis of hydrological disasters because the relative importance of one variable (social or hydrological) over another is uncertain. Thus, comparison of storm scenarios derived from a swing-weight technique reveals the sensitivity of the system to both single and multiple variables input into the model.

The disruption of tropical cyclone disaster scenarios compared to the baseline order is mapped to identify basins of top priority and basins of greatest change in priority. The sum of squares of differences in order of basins relative to the baseline order is used to identify scenarios that are most and least disruptive. A regional demonstration of this approach with features of Hurricane Ian is provided. The approach is an example of multidisciplinary innovation toward providing high-resolution risk communication to disaster managers and policymakers for systems analysis and resource allocation. The maps and other results can inform priorities and strategies aimed to decrease or transfer tropical cyclone risk and improve system resilience within basins of high tropical cyclone exposure and high social vulnerability.

Hurricane lan Damages

In September 2022, Hurricane Ian became the third costliest hurricane in US history with more than \$114 billion in estimated damage (Smith 2023; Smith and Katz 2013). Hurricane Ian caused 156 direct and indirect fatalities, 150 of which occurred in Florida, making this the deadliest storm in Florida since 1935 (Bucci et al. 2022; Karimiziarani and Moradkhani 2023).

Conditions for Hurricane Ian were described by the National Oceanic and Atmospheric Administration (NOAA) National Hurricane Center and the media as *catastrophic*, *life-threatening*, and *deadly* (Bucci et al. 2022). Damages included, but were not limited to, storm surge up to 5 m above ground level, extensive flooding, destruction and damage to infrastructure, multiple tornadoes, and tropical-storm force winds (Bucci et al. 2022). Hundreds of water rescues were necessary, and an estimated 9.62 million people were without power (Bucci et al. 2022). In the aftermath of Ian, receding stormwater transported pollutants and debris to the Gulf of Mexico, which caused harmful algal blooms off the Florida coast (Bucci et al. 2022).

Hurricane Ian Meteorology

Ian originated off the west coast of Africa, rapidly intensified in warm Atlantic Ocean water, and made its first landfall in western Cuba as a Category III hurricane on the Saffir-Simpson Hurricane Wind Scale on September 27 (Bucci et al. 2022). The system continued into the Gulf of Mexico, where it strengthened to a brief peak intensity of a Category V hurricane (Bucci et al. 2022). Ian weakened slightly to a Category IV hurricane before making landfall near Punta Gorda, Florida, on September 28 (Bucci et al. 2022). As Ian slowly traversed Florida, it weakened to tropical storm status before reentering the Atlantic Ocean near Cape Canaveral, Florida, on September 29 (Bucci et al. 2022). Once in the Atlantic Ocean, Ian intensified to a Category I hurricane and made its final landfall near Georgetown, South Carolina. Ian gradually weakened in the Carolinas and dissipated on October 1 (Bucci et al. 2022).

Hurricane Ian Data Collection

Numerous data collection methods were employed before, during, and after Hurricane Ian to support forecasting, response, and recovery efforts. For example, data were collected using ground-based weather radars, networks of buoys, dropwindsonde observations, satellite observations, Hurricane Hunter flights, and meteorological/environmental models (Bucci et al. 2022). It is important to note that during Hurricane Ian's landfall in the US, many in situ observation stations suffered instrument failures due to their exposure to the hurricane and were unable to capture the peak meteorological

conditions (Bucci et al. 2022). Thus, satellite-based Earth observations provide a valuable contribution to hurricane data collection by providing high-resolution spatial and temporal data during the disaster that could have been unobservable otherwise.

Hurricane Ian Social Vulnerability Challenges

Forecast and warnings for Hurricane Ian were issued 39-48 h in advance of its landfall in both Florida and South Carolina (Bucci et al. 2022). Even with relatively good forecasting and early issues of warnings, as was the case with Hurricane Ian, previous studies have shown that social vulnerability factors decrease the ability of individuals to safely evacuate (Anand et al. 2023; Flanagan et al. 2011, 2018; Meyer et al. 2018). Social vulnerability may explain the high number of fatalities during Hurricane Ian, particularly considering that reports of indirect causes of death included lack of access to timely medical care, accidents (such as falling during power outages), cardiac events, etc. (Bucci et al. 2022). Additionally, the elderly composed the highest proportion of fatalities during Hurricane Ian, which is generally observed during disasters (Bucci et al. 2022; Flanagan et al. 2011).

Geographic Area of the Demonstration

The NOAA National Weather Service estimates of Hurricane Ian's path and wind swath over the contiguous United States were used to define a study area of 922 subbasins within and traversing portions of the following five southeastern states: Alabama, Florida, Georgia, North Carolina, and South Carolina (Fig. 1). The subbasins were defined using the Level 08 HydroBASINS product (Lehner and Grill 2013). The study area encompassed approximately 700,000 km².

A digital elevation model (DEM) for the study area is shown in Fig. 1(a) and was derived from the National Aeronautics and Space Administration (NASA) Shuttle Radar Topography Mission (SRTM). Due to the variability of low-lying terrain and the Appalachian Mountains, elevation within the study area ranged from approximately -29 to +1,977 m relative to mean sea level (MSL). The mean elevation was +145 m MSL.

Sources of Data for the Demonstration

Descriptions of data used in this study for social factors (i.e., SVI) and hydrology factors (i.e., precipitation, wind speed, and soil moisture) are provided in the following subsections. Table 1 summarizes the temporal resolution, native spatial resolution, resampled resolution, resampling method, study period, and source for each data set.

Subbasin Delineations from HydroBASINS

HydroBASINS, a secondary data set of the World Wildlife Fund's HydroSHEDS product, provides hierarchical subbasin boundaries at a global scale (Lehner and Grill 2013). For this demonstration, the Level 08 HydroBASINS product is used because it is the finest subbasin resolution, which guarantees at least one unique Earth observation pixel per subbasin. In total, the study area has 922 subbasins with a mean area of 748 km² and a median area of 533 km². Additional details of HydroBASINS are available in Appendix III (HydroSHEDS, n.d.).

CDC/ASTDR Social Vulnerability Index

Social vulnerability data are obtained from the Center for Disease Control and Prevention Agency for Toxic Substances and Disease Registry Social Vulnerability Index (CDC/ASTDR SVI, henceforth referred to as SVI). This data set provides vulnerability estimates at the United States Census Tract level for select years between 2000 and 2020 (CDC/ATSDR 2023). The US wide SVI product for 2020 is used to allow for multistate analyses and since it was the most up-to-date version available at the time of this study.

A summary of 16 variables contributing to overall SVI calculations is provided in Appendix II. SVI indices range from 0 to 1, with 1 indicating the most vulnerable and 0 indicating the least

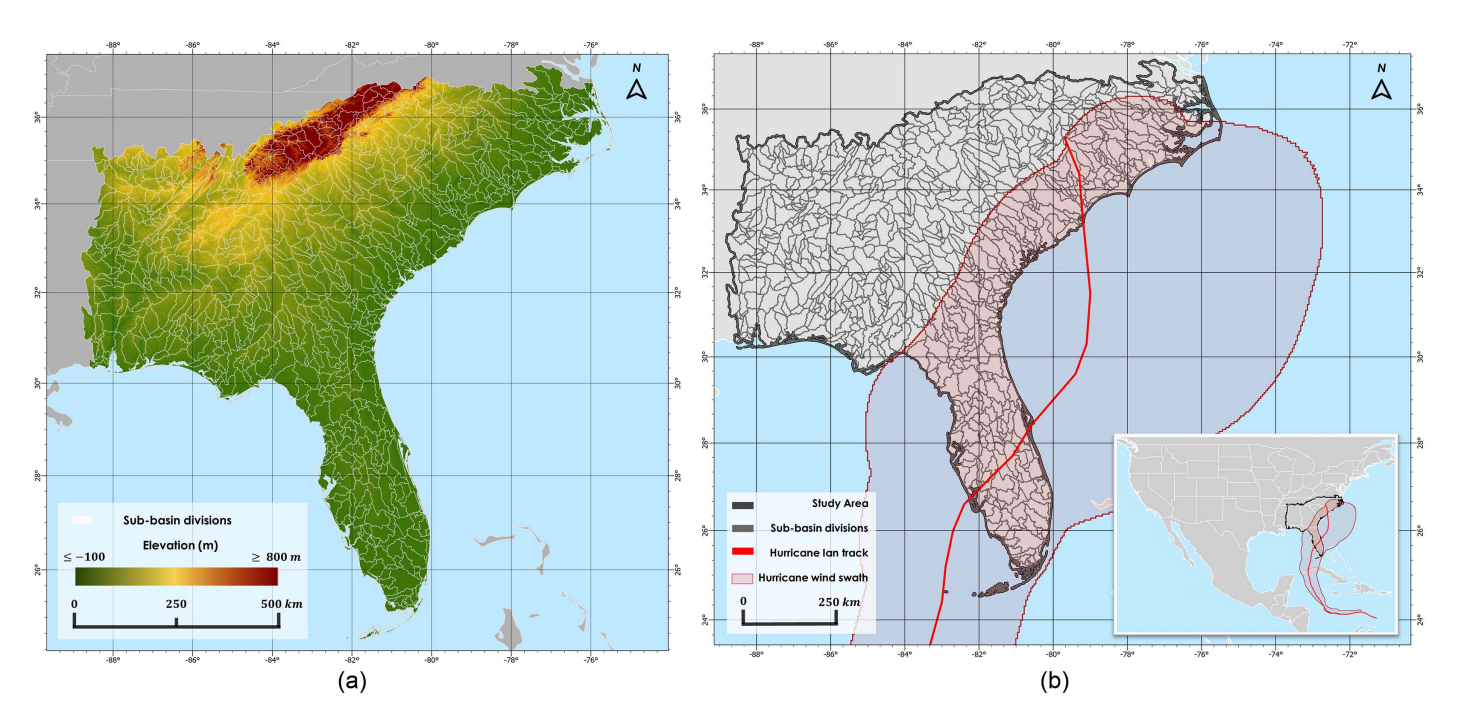


Fig. 1. Area of demonstration within the Southeastern United States: (a) digital elevation model (DEM) and HydroBASINS Level-08 subbasins; and (b) hurricane Ian track and wind swath estimates from NOAA National Weather Service and HydroBASINS Level-08 subbasins.

Table 1. Summary of hydrology and social vulnerability data used in this study, including the variable, sensor/model, native spatial resolution, resampled resolution, resampling method, temporal resolution, study period, and sources

Variable	Sensor/model	Native spatial resolution	Resampled resolution	Resampling method	Temporal resolution	Study period	References
Social vulnerability index (SVI)	CDC/ATSDR social vulnerability index 2020 database, US	Census tracks	Level 08 Hydro-BASINS	Spatial average	1 year	2020	CDC/ATSDR (2023)
Precipitation	GPM IMERG late precipitation L3 half hour precipitation V06	0.1°	Level 08 Hydro-BASINS	Spatial sum and spatial maximum	1 h	September 27– October 1, 2022	Huffman et al. (2020)
Soil moisture (near-surface, 0–5 cm)	UVA 1-km downscaled soil moisture product	1-km	Level 08 Hydo-BASINS	Spatial average	12 h	September 23– September 27, 2022	Lakshmi and Fang (2023)
Wind speed	ECMWF ERA5	0.25°	Level 08 Hydro-BASINS	Spatial maximum	1 h	September 27– October 2, 2022	Hersbach et al. (2020)
Subbasins	HydroBASINS	Level 08	N/A	N/A	N/A	N/A	Lehner and Grill (2013)

vulnerable regions. Additional details of the SVI data are available in Appendix II (CDC/ASTDR 2023).

Precipitation Data from GPM IMERG

Precipitation data are derived from the Integrated Multi-satellitE Retrievals for Global Precipitation Measurement (GPM IMERG) missions, which provide up to half-hourly precipitation observations at a spatial resolution of 0.1° (Huffman et al. 2020).

For this study, the GPM IMERG Late Precipitation V06 Half Hour Precipitation data set from September 27 to October 2, 2022, is used to calculate maximum hourly precipitation (i.e., precipitation intensity) and cumulative precipitation (i.e., precipitation duration). Additional information for GPM IMERG is available in Appendix III (NASA, n.d.).

Wind Speed Data from ECMWF ERA5

Wind speed data were obtained from the Copernicus Climate Change Service (C3S) European Centre for Medium-Range Weather Forecast (ECMWF) Reanalysis Version 5 (ERA5). For this study, hourly wind speed data from September 27 to October 2, 2022, are calculated using Eq. (1), where u is the u-component of wind in the longitudinal direction 10 m above the surface of the Earth and v is the v-component of wind in the latitudinal direction 10 m above the surface of the Earth. Both u and v are utilized at hourly temporal resolutions:

Wind speed =
$$\sqrt{u^2 + v^2}$$
 (1)

Additional information for ERA5 is available in Appendix III (ECMWF, n.d.).

SMAP-Derived 1-km Downscaled Surface Soil Moisture Product

The soil moisture active passive (SMAP) derived 1-km downscaled surface soil moisture product is used to calculate the 5-day antecedent near-surface soil moisture (0–5 cm depth below the surface of the Earth) (Lakshmi and Fang 2023). For this study, antecedent soil moisture is examined because of fallen tree damage reports during Hurricane Ian attributed to saturated soil, high winds, and widespread flooding (Bucci et al. 2022). The study period of September 23–27, 2022, provided 5-day antecedent soil moisture

data prior to landfall of Hurricane Ian in Florida. This was the shortest antecedent period with sufficient observational coverage since the data set is limited by cloud cover. Additional details on the SMAP-derived 1-km downscaled surface soil moisture product are available in Appendix III (NSIDC, n.d.).

Methods

This section describes the methodology in several parts as follows: first, all variables are resampled to a subbasin scale as defined by the Level 08 HydroBASINS data set. Second, the subbasins are characterized from highest to lowest order for each variable. Third, the basin order using SVI is defined as the baseline scenario, which represents initial conditions of the study area prior to the hurricane disturbance. Fourth, storm scenarios are defined based on the hydrology and SVI variables. Fifth, a swing-weight technique is used to update factor weights for each scenario. Sixth, risk is calculated for each scenario as the difference in basin order of the baseline scenario versus a given scenario. Seventh, a score of disruptiveness is calculated for each scenario using the normalized sum of squares of differences in order. Further details of each step are provided in the subsequent paragraphs.

Hydrology and social vulnerability variables are first resampled to each subbasin (defined by the Level 08 HydroBASINS data set) to allow for comparisons regardless of the native resolution of each data set. For SVI and 5-day antecedent soil moisture (SM), a spatial average is used. For cumulative precipitation (P1), a spatial sum is used. For maximum hourly precipitation (P2) and maximum hourly wind speed (W), a spatial average of maximum observed values is used. Fig. 2 provides spatial plots of the original resampled variables.

The subbasins are then characterized by ordering from highest to lowest value and assigning an integer value from 1 to the total number of basins using Eq. (2):

$$S_n(b_i) = 100 \times \sum_{j=1}^k w_j v_{ij}$$
where $\left\{ w_j \middle| \sum_{j=1}^k w_j = 1, \quad 0 \le w_j \le 1, \ j = 1, \dots, k \right\}$

where the basin order for the *i*th basin (b_i) under the *n*th scenario (S_n) is defined as the summation of j to k variables for

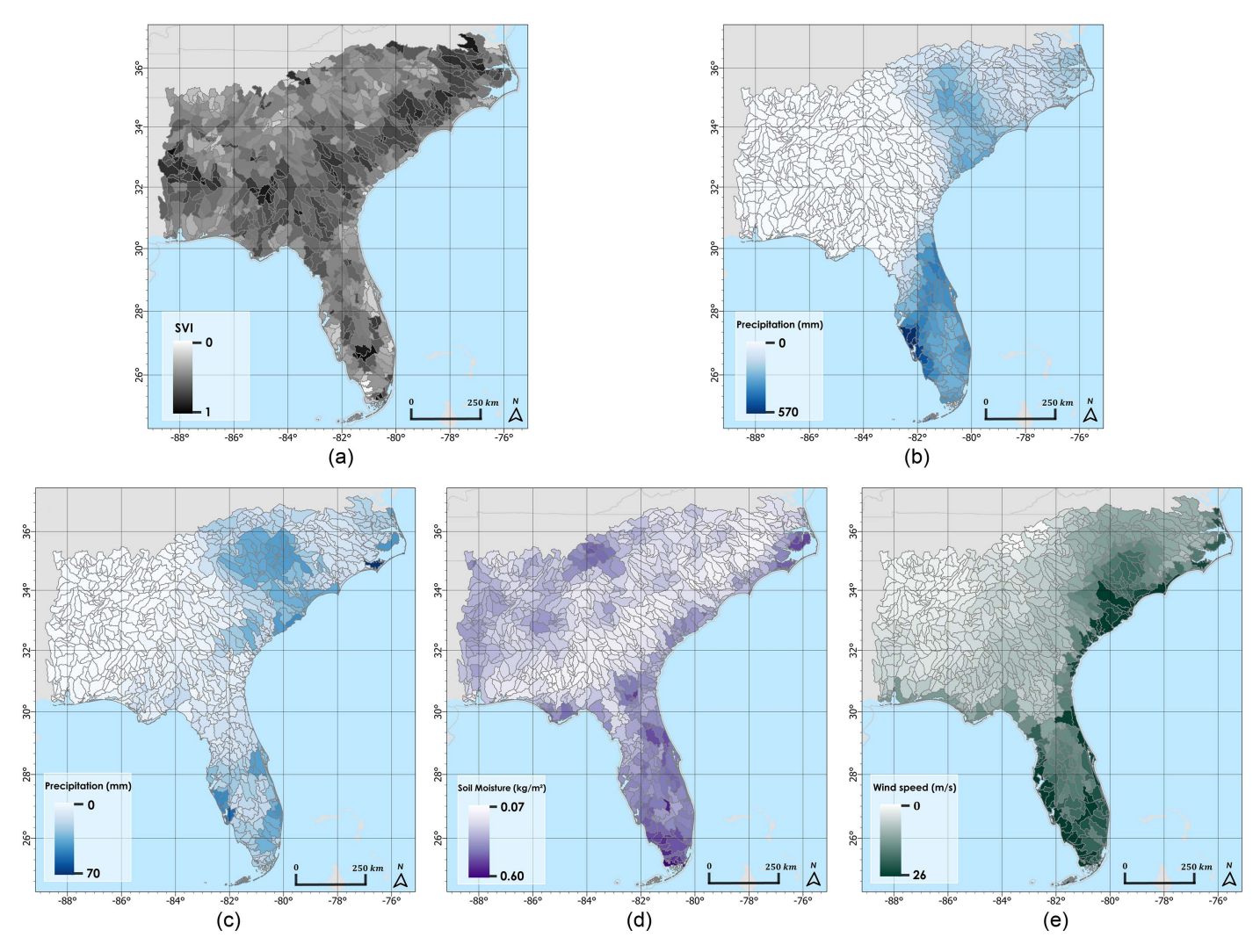


Fig. 2. Spatial maps of the observed social vulnerability and hydrology variables resampled per subbasin for (a) social vulnerability index; (b) cumulative precipitation; (c) maximum hourly precipitation; (d) 5-day antecedent soil moisture; and (e) maximum hourly wind speed.

the *i*th basin (v_i) multiplied by the *j*th defined weight (w_i) . For example, the basin with the most observed cumulative precipitation during Hurricane Ian has an order value of 1, whereas the basin with the least observed cumulative precipitation will have an order of 922 (the maximum value of i).

Then, the swing-weight technique is used to update factor weights for each of the 20 scenarios for the study. As previously mentioned, the swing-weight technique allows for tradeoffs of higher consideration of one or more variables in exchange for lower consideration of other variables within a scenario. Table 2 summarizes the scenarios and weights for each hydrology and social vulnerability variable. Scenarios using a single variable are S1-S5. Scenarios using a combination of variables (up to five in total) are S6–S20. The *uncertainty* is addressed by the identification of the several scenarios, without assessing probabilities. Subsequently the risk is quantified as of the degree of disruption of system order by each of the scenarios (Hassler et al. 2019). Since the motivation of this study is to understand the extent by which hydrological extremes disrupt social vulnerability, S1 is defined as the baseline order as it exclusively uses SVI and is assumed to represent conditions prior to the hurricane disturbance. For S6-S20, a constant SVI weight of 0.5 was used. This ensures a balance between SVI and the hydrological contributions within each new order calculation, as well as equal contributions of SVI across the remaining scenarios.

For each scenario, we define risk (R) as the difference between the baseline order and scenario order for a given basin using Eq. (3):

$$R_n(b_i) = B(b_i) - S_n(b_i) \tag{3}$$

In Eq. (3), the risk of a given scenario and basin $R_n(b_i)$ equals the difference between the baseline order of the basin $B(b_i)$ and the scenario order of the basin $S_n(b_i)$. A positive value for R indicates the basin increased in order due to the disruption. A negative Rindicates the basin decreased in order following the disruption. For the demonstration of Hurricane Ian, a positive value for Rwould occur for a basin with low SVI and high hydrological exposure. A negative value for R would occur for a basin with high SVI and low hydrological exposure. A near-zero R would occur for a basin either with high SVI and high hydrological exposure or a basin with low SVI and low hydrological exposure. Spatial plots of scenario basin orderings $S_n(b_i)$ and risk $R_n(b_i)$ are used to examine spatial patterns of social vulnerability and hydrology across the study area.

Table 2. A swing-weight technique is used to update factor weights for each of the 20 scenarios of the contributing hydrology and social vulnerability variables

	Swing v	veights (w _j)) of contrib	uting varial	oles (v_j)
Scenario (S_n)	v_1 : SVI	<i>v</i> ₂ : P1	v ₃ : P2	v ₄ : W	<i>v</i> ₅ : SM
S_1 : SVI (baseline order)	1	0	0	0	0
S_2 : Hurricane Ian cumulative precipitation	0	1	0	0	0
S_3 : Hurricane Ian maximum hourly precipitation	0	0	1	0	0
S_4 : Hurricane Ian maximum hourly wind speed	0	0	0	1	0
S_5 : Hurricane Ian 5-day antecedent soil moisture	0	0	0	0	1
S_6 : SVI and Hurricane Ian cumulative precipitation	0.5	0.5	0	0	0
S_7 : SVI and Hurricane Ian maximum hourly precipitation	0.5	0	0.5	0	0
S_8 : SVI and Hurricane Ian maximum hourly wind speed	0.5	0	0	0.5	0
S_9 : SVI and Hurricane Ian 5-day antecedent soil moisture	0.5	0	0	0	0.5
S_{10} : SVI, Hurricane Ian cumulative precipitation and maximum hourly precipitation	0.5	0.25	0.25	0	0
S_{11} : SVI, Hurricane Ian cumulative precipitation and maximum hourly windspeed	0.5	0.25	0	0.25	0
S_{12} : SVI, Hurricane Ian cumulative precipitation and 5-day antecedent soil moisture	0.5	0.25	0	0	0.25
S_{13} : SVI, Hurricane Ian maximum hourly precipitation and maximum hourly wind speed	0.5	0	0.25	0.25	0
S_{14} : SVI, Hurricane Ian maximum hourly precipitation and 5-day antecedent soil moisture		0	0.25	0	0.25
S_{15} : SVI, Hurricane Ian maximum hourly wind speed and 5-day antecedent soil moisture	0.5	0	0	0.25	0.25
S_{16} : SVI, Hurricane Ian cumulative precipitation, maximum hourly precipitation, and maximum hourly wind speed	0.5	0.167	0.167	0.167	0
S_{17} : SVI, Hurricane Ian cumulative precipitation, maximum hourly precipitation, and 5-day antecedent soil moisture	0.5	0.167	0.167	0	0.167
S_{18} : SVI, Hurricane Ian cumulative precipitation, maximum hourly wind speed, and 5-day antecedent soil moisture	0.5	0.167	0	0.167	0.167
S_{19} : SVI, Hurricane Ian maximum hourly precipitation, maximum hourly wind speed, and 5-day antecedent soil moisture	0.5	0	0.167	0.167	0.167
S_{20} : SVI, Hurricane Ian cumulative precipitation, maximum hourly precipitation, maximum hourly wind speed, and 5-day antecedent soil moisture	0.5	0.125	0.125	0.125	0.125

Note: Contributing variables include social vulnerability index (SVI), cumulative precipitation (P1), maximum hourly precipitation (P2), maximum hourly wind speed (W), and 5-day antecedent soil moisture (SM).

Lastly, the most and least disruptive scenarios were determined using the normalized sum of squares of differences in order, as in Eqs. (4) and (5):

$$x(S_n) = \sum_{i=1}^{N} (B(b_i) - D(b_i))^2 = \sum_{i=1}^{N} R(b_i)^2$$
 (4)

$$X(S_n) = \frac{x(S_n) - x(S)_{min}}{x(S)_{max} - x(S)_{min}}$$
(5)

In Eq. (4), $x(S_n)$ represents the score of disruptiveness for a given scenario (S_n) as the sum over the basins of the squared differences of the baseline order and disrupted order. This calculation quantifies risk as an influence of each scenario to the system order (Bonato et al. 2022; Karvetski et al. 2009; You et al. 2014). The normalized score of disruptiveness $[X(S_n)]$ is calculated [Eq. (5)] as the score of disruptiveness for a given scenario $x(S_n)$ minus the minimum score of disruptiveness $[x(S)_{min}]$ divided by the maximum score of disruptiveness $[x(S)_{max}]$ minus the minimum score of disruptiveness $[x(S)_{min}]$. The least disruptive scenario had the lowest normalized score of disruptiveness. The most disruptive scenario had the highest normalized score of disruptiveness.

Sample of Results

The results and discussion are organized into the following subsections: (1) single variable basin order results; (2) scenario results; (3) basin ordering for select scenarios; and (4) basin risk for select scenarios. For each of the variables and scenarios, lower order/percentiles indicate greater concern and thus might be prioritized

for near-term disaster recovery, response, and future mitigation efforts.

Single Variable Basin Order Results

Social Vulnerability Index Order

As previously discussed, the SVI order shown in Fig. 2(a) was defined as the baseline order for this study. Even though SVI is based on a national scale, a wide distribution of SVI was observed in the study area with a minimum of 0.005, maximum of 0.974, mean of 0.548, and median of 0.576 [Fig. 3(a)]. The spatial plot of SVI order in Fig. 4(a) shows that the lowest order SVI basins are concentrated in the southeastern portions of Alabama, Georgia, South Carolina, and North Carolina.

Coastal basins tended to have higher order compared to adjacent inland basins. This indicates that inland basins have populations with more social vulnerability than coastal basins. This is particularly apparent in Florida and may be explained by recent trends of increased demand for 'coastal lifestyle housing' observed by Florida real estate agents (Palm and Bolsen 2023).

Precipitation (P1 and P2) Orders

Precipitation is separately analyzed as cumulative precipitation (mm, P1) and maximum hourly precipitation rate (mm/h, P2) to account for both precipitation intensity and duration.

Fig. 3(b) shows a histogram of total precipitation within the study area. Fig. 3(b) shows the spatial distribution of basin ordering based on cumulative precipitation. While little to no precipitation is observed in the western portion of the study area, basins located within the path of Hurricane Ian were exposed to extreme precipitation amounts of up to 500 mm within the 6-day period. The mean and median cumulative precipitation are, respectively,

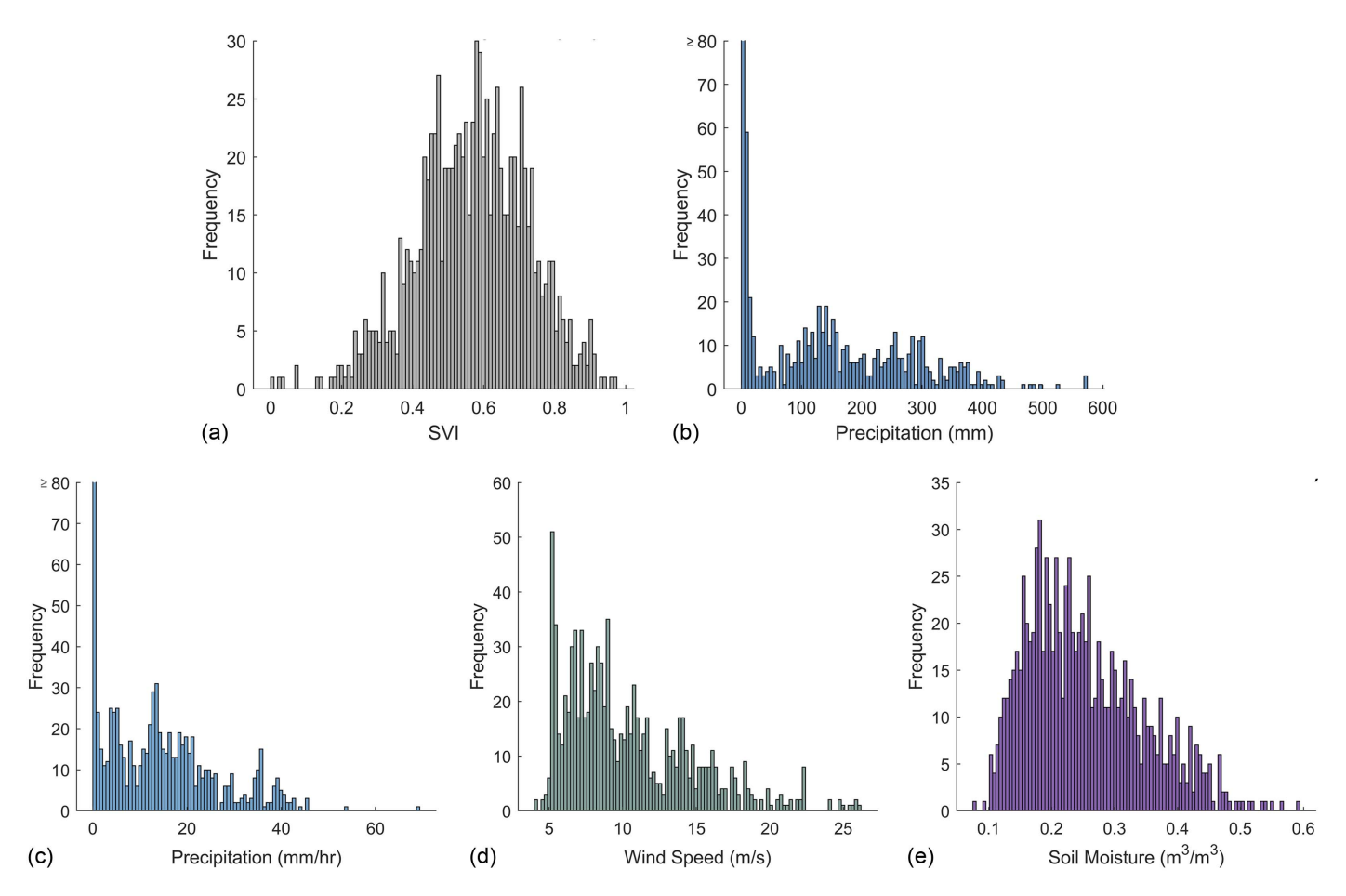


Fig. 3. Histograms of the observed social vulnerability and hydrology variables resampled per subbasin in the area of demonstration for (a) social vulnerability index (SVI); (b) total precipitation; (c) hourly maximum precipitation; (d) hourly maximum wind speed; and (e) 5-day antecedent soil moisture.

31 and 104 mm. The highest prioritization of basins follows the path of Hurricane Ian over Central Florida and South Carolina. Cumulative precipitation order is higher in Florida than in the Carolinas. This is likely due to the duration of the hurricane's presence over Florida because the system was relatively slow-moving and took approximately 16 h for the eyewall to pass from Florida's Gulf Coast to the Atlantic Coast (Bucci et al. 2022). In the Carolinas, it took approximately 6 h for the system to transition to an extratropical cyclone after making landfall (Bucci et al. 2022).

Hourly maximum precipitation (P2) exhibited a similar distribution to the cumulative precipitation, particularly with western basins of the study period observing little to no precipitation rates [Fig. 3(c)]. A wide distribution of precipitation rates was observed with a maximum of 69 mm/h, mean of 12 mm/h, and median of 10.6 mm/h [Fig. 3(c)]. The spatial order plot of maximum hourly precipitation showed the highest prioritization of basins in the Carolinas, followed by Florida [Fig. 4(c)]. This indicates that the Carolinas were exposed to more intense rainfall than Florida, despite the greater cumulative precipitation observed in Florida.

Wind Speed (W) Order

The distribution of maximum hourly wind speed in Fig. 3(d) shows the study area was exposed to varying wind speeds from a minimum of 4.2 m/s to a maximum of 26.1 m/s. The median and mean wind speeds are, respectively, 9.0 m/s and 10.3 m/s. In the spatial order plot of maximum hourly wind speed shown in Fig. 4(e); coastal basins tend to be higher priority than inland basins. This is expected because of coastal convection processes. However, the inland basins of Florida and the Carolinas tended to exhibit higher prioritization over other basins outside of the path of Hurricane Ian.

Soil Moisture Order

Fig. 3(e) shows the distribution of 5-day antecedent soil moisture, which had a minimum of 0.8 m³/m³, a maximum of 0.59 m³/m³, a mean of $0.25 \text{ m}^3/\text{m}^3$, and a median of $0.24 \text{ m}^3/\text{m}^3$. In this study, higher soil moisture is prioritized because soil with a high degree of water saturation has less pore space readily available to store additional water. When exposed to extreme precipitation events, the decreased pore capacity to store water can result in flooding because the volumetric water content of the soil increases to its porosity, rendering it saturated.

The spatial plot of ordered 5-day antecedent soil moisture shown in Fig. 4(d) reveals that the highest priority soil moisture values are observed in Florida and coastal basins. Notably, the lowest soil moisture values are opposite to the spatial distribution of SVI order; basins of high SVI tend to be colocated with basins of low soil moisture in the noncoastal basins of southern Alabama, Georgia, South Carolina, and North Carolina. Future research should be dedicated to comparing the spatial and temporal distributions of SVI and soil moisture using a longer study period and national scale. This would improve understanding of whether the inverse relationship of SVI and soil moisture observed in this study is correlated or coincidental.

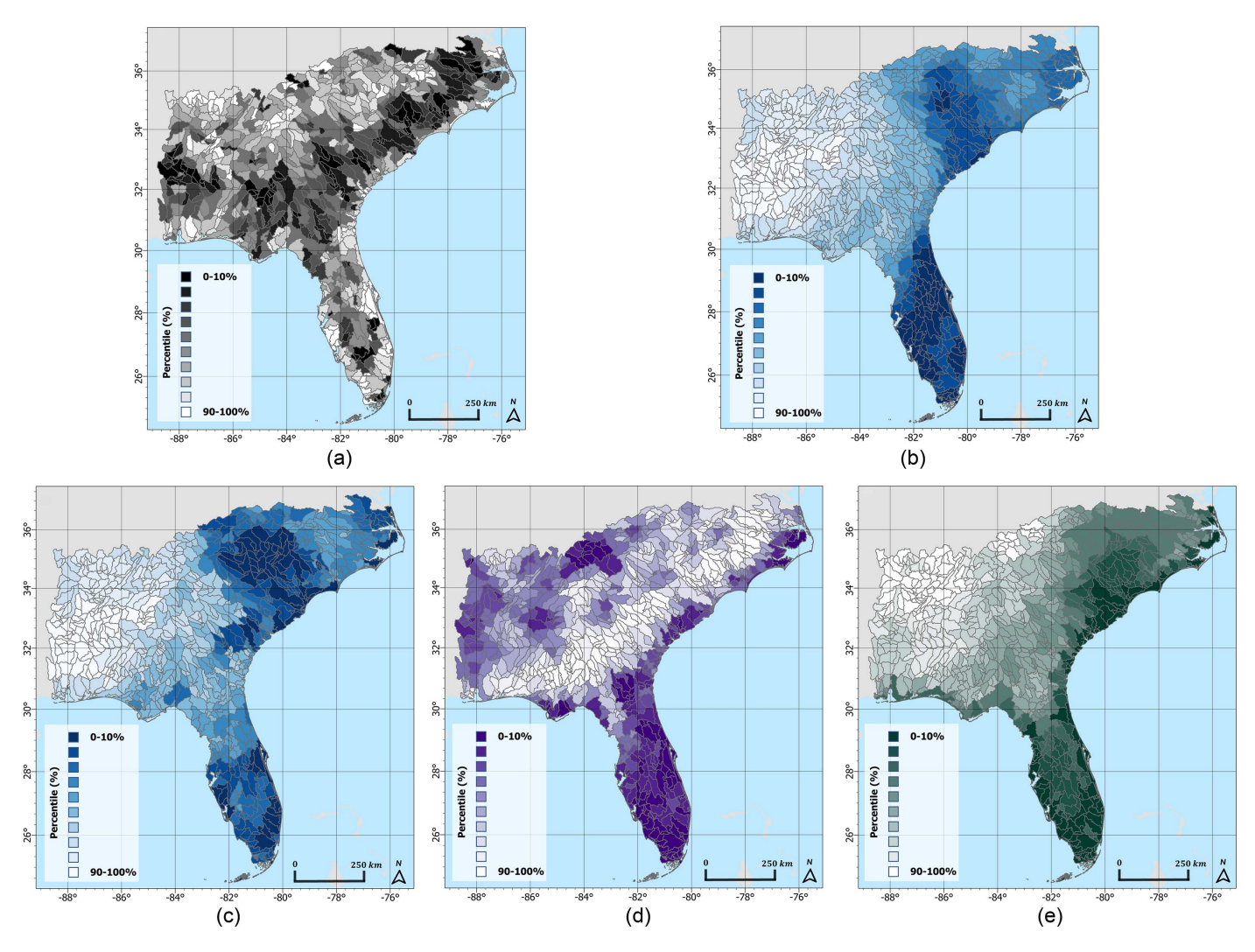


Fig. 4. Maps of the ordered percentiles within the area of demonstration at the subbasin level for the following social vulnerability and hydrology variables: (a) social vulnerability index (SVI); (b) cumulative precipitation; (c) maximum hourly precipitation; (d) 5-day antecedent 1-km soil moisture; and (e) maximum hourly wind speed.

Scenario Results

To further investigate basin sensitivity to each scenario, the average order of the top 10% of basins (92) from S_{20} is plotted across all scenarios (S_1 – S_{20}) in Fig. 5. When only one variable was used to define a scenario (S_1 – S_5), a wide distribution of average orders was observed. As more variables contributed to a given scenario (three variables for S_{10} – S_{15} , four variables for S_{16} – S_{19} , and five variables for S_{20}), the overall average basin orders stabilized and exhibited less variability of order compared to scenarios with one to two variables.

Notable peaks in order occurred during S_5 and S_9 , both of which relied on the 5-day antecedent soil moisture data for ordering. This indicates that the soil moisture data contributes different ordering priorities compared to the other variables, likely because it was the only hydrology variable observed prior to the hurricane event. However, when two or more variables contribute to a scenario in combination with the 5-day antecedent soil moisture data, the peaks are not pronounced. Thus, incorporating multiple hydrology variables into a given scenario is important to reduce basin sensitivity to an individual variable and to improve representation of exposure to the extreme hydrological event.

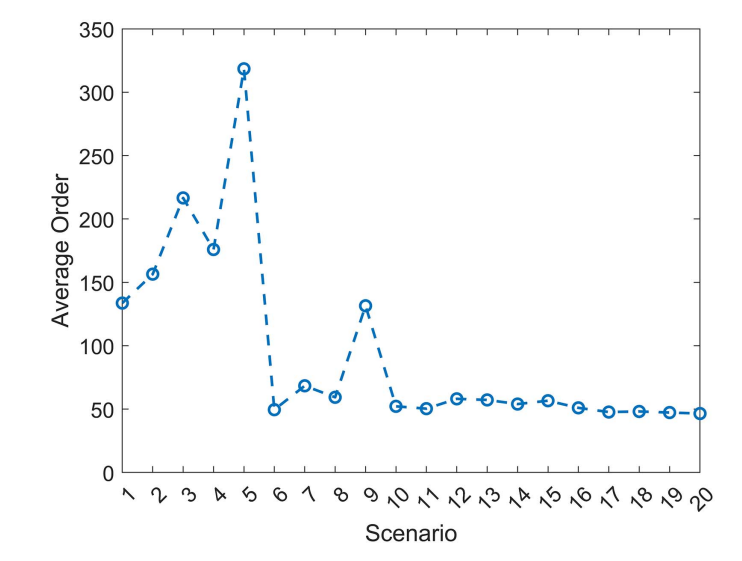


Fig. 5. Average order of the top 10% of basins from scenario S_{20} across all scenarios (S_1 – S_{20}). The overall ordering stabilizes as more hydrology and social vulnerability variables contribute to a given scenario.

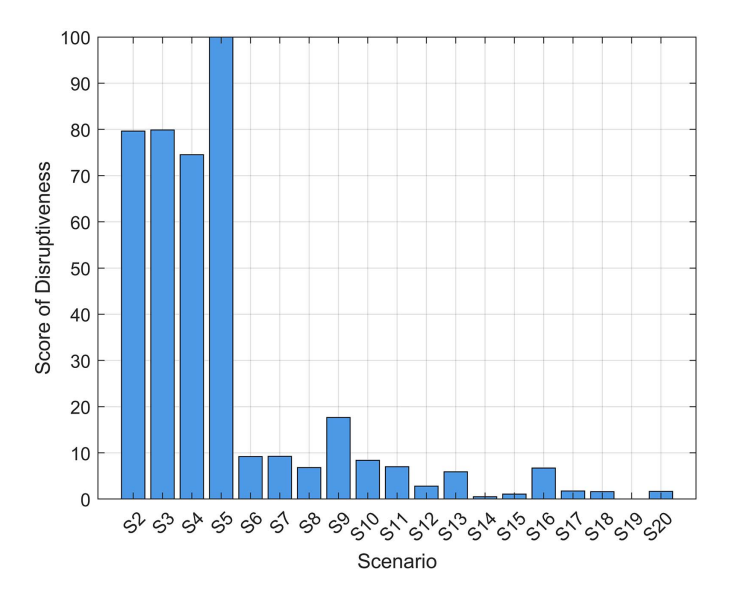


Fig. 6. Normalized score of disruptiveness for scenarios $(S_2 - S_{20})$ to determine the most and least disruptive scenarios compared to the baseline SVI order (S₁).

Fig. 6 shows a bar graph of the normalized score of disruptiveness for each scenario, which was calculated using Eqs. (4) and (5). The most disruptive scenarios were S₅ (Hurricane Ian 5-day antecedent soil moisture), S₃ (Hurricane Ian maximum hourly precipitation), and S2 (Hurricane Ian cumulative precipitation) because they exhibited the highest normalized scores of disruptiveness. Each of these scenarios had only one contributing variable with different spatial orderings compared to the baseline order, resulting in the highest disruption. The least disruptive scenarios, exhibiting the lowest normalized scores of disruptiveness, were S₁₉ (SVI, Hurricane Ian maximum hourly precipitation, maximum hourly wind speed, and 5-day antecedent soil moisture) and S₁₄ (SVI, Hurricane Ian maximum hourly precipitation and 5-day antecedent soil moisture). These scenarios accounted for three and four hydrology and social vulnerability factors, resulting in basin ordering that

were least different from the baseline order compared to the other scenarios.

Table 3 describes the disruption of order of basins across scenarios compared to the baseline order, using 10% increments of disruption. Similar to Figs. 5 and 6, the most disruptive scenarios are S2, S3, S4, and S5 since each hydrology variable individually orders the basins dissimilarly to SVI. Scenario S₅ has the fewest number of basins in the 0%-10% disruption category indicating that antecedent soil moisture ordering differed the greatest from the SVI order. As previously noted, this disruption may indicate that low soil moisture corresponds to regions of high social vulnerability but would require additional research to confirm whether this is correlated or coincidental.

Across all scenarios, disruptions of basin order are at least 50% (Table 3). Scenarios S_{19} and S_{14} were previously identified as the least disruptive scenarios (Fig. 6) with no basin disruptions greater than 50% (Table 3). For S₁₉, 37% of the study area (343 basins) had 0%-10% disruption, 33% (310 basins) had 10%-20% disruption, 19% (179 basins) had 20%-30% disruption, 6% (61 basins) had 30%–40% disruption, and 3% (29 basins) had 40%–50% disruption. For S_{14} , 40% of the study area (371 basins) had 0%–10% disruption, 29% (271 basins) had 10%-20% disruption, 20% (180 basins) had 20%-30% disruption, 8% (71 basins) had 30%-40% disruption, and 3% (29 basins) had 40%-50% disruption.

Basin Ordering for Select Scenarios

Spatial plots of the basin ordering are provided in Fig. 7 to investigate spatial patterns of the following three selected scenarios: (1) the most disruptive scenario that includes both social vulnerability and hydrology (S₉); (2) the most disruptive scenario that includes social vulnerability and three or more hydrology variables (S_{16}) ; and (3) the least disruptive scenario (S_{19}) . Even though each scenario has a unique basin ordering spatial map, these three selected scenarios (S₉, S₁₆, S₁₉) adequately represent the range of basin orders and risk across the scenarios and thus are provided in this manuscript.

Fig. 7(a) shows the basin ordering of the most disruptive scenario, S₉, which was defined as equal contributions of SVI and 5-day antecedent soil moisture. Basins of the lowest order are found

Table 3. Summary of the number of basins within 10% increments of disruption across scenarios S_2 - S_{20} compared to the baseline order (S_1)

Scenario	Number of basins within a percentage of disruption (%) compared to S_1									
(S_n)	0%-10%	10%-20%	20%-30%	30%-40%	40%-50%	50%-60%	60%-70%	70%-80%	80%-90%	90%-100%
$\overline{S_2}$	196	176	127	101	107	70	53	39	33	20
S_3	196	169	128	111	97	80	49	39	34	19
S_4	210	178	122	109	109	63	52	31	29	19
S_5	166	130	115	118	113	92	75	53	42	18
S_6	308	269	167	94	84	0	0	0	0	0
S_7	300	274	165	110	70	3	0	0	0	0
S_8	322	262	173	104	59	2	0	0	0	0
S_9	263	217	182	144	104	12	0	0	0	0
S_{10}	289	297	154	117	65	0	0	0	0	0
S_{11}	326	249	166	126	55	0	0	0	0	0
S_{12}	368	269	164	69	51	1	0	0	0	0
S_{13}	327	254	181	117	43	0	0	0	0	0
S_{14}	371	271	180	71	29	0	0	0	0	0
S_{15}	387	259	168	69	38	1	0	0	0	0
S_{16}	312	271	174	108	57	0	0	0	0	0
S_{17}	320	308	186	80	28	0	0	0	0	0
S_{18}	348	294	176	66	38	0	0	0	0	0
S_{19}	343	310	179	61	29	0	0	0	0	0
S_{20}	335	274	203	80	30	0	0	0	0	0

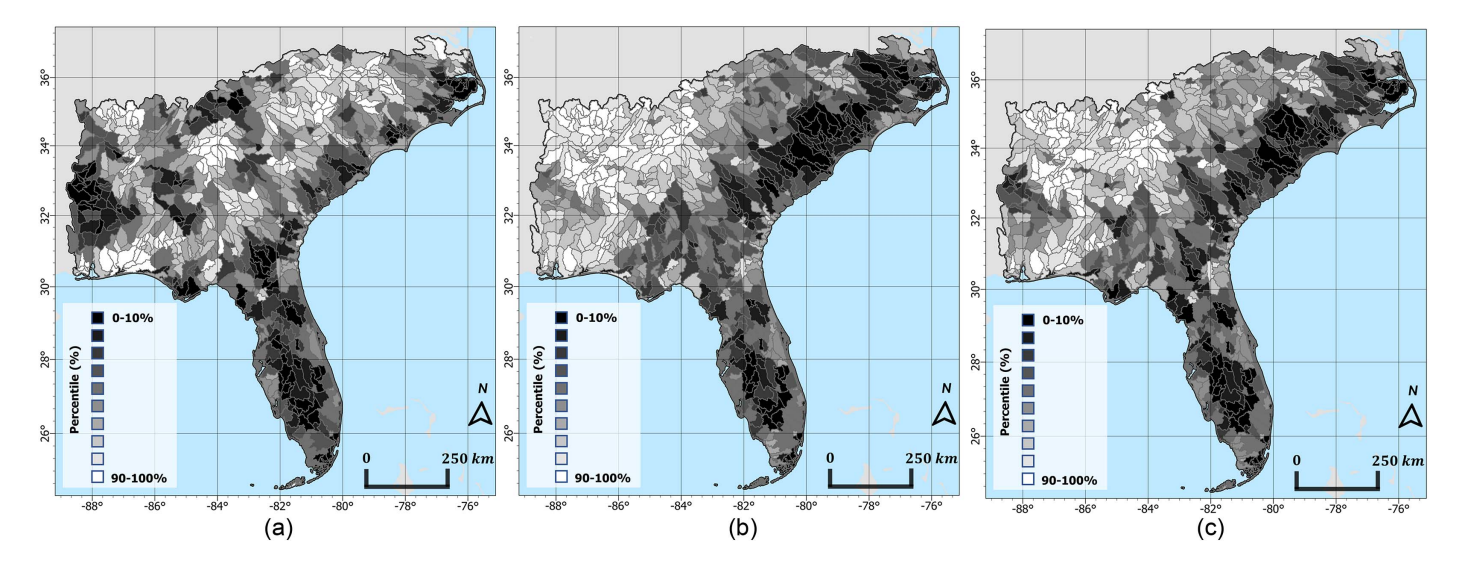


Fig. 7. Spatial plot of the basin ordering for the following scenarios: (a) S_9 —SVI and Hurricane Ian 5-day antecedent soil moisture; (b) S_{16} —SVI, Hurricane Ian maximum cumulative precipitation, maximum hourly precipitation, and maximum hourly wind speed; and (c) S_{19} —SVI, Hurricane Ian maximum hourly precipitation, maximum hourly wind speed, and 5-day antecedent soil moisture.

in western Alabama and inland Florida because they had both high soil moisture and social vulnerability.

For scenarios S_{16} [Fig. 7(b) and S_{19} Fig. 7(c)], the lowest order basins were found in Central Florida and the southeastern portions of the Carolinas. This is consistent with the first landfall of Hurricane Ian in Florida and its second landfall in South Carolina. Conversely, the highest order basins occurred safely beyond the path of Hurricane Ian in Alabama, northern Georgia, and the northwestern portions of the Carolinas.

Surprisingly, coastal basins within the path of Hurricane Ian exhibited higher order than their adjacent inland basins, even though the single variable basin ordering (Fig. 4) reveals that coastal basins

Table 4. Summary of top-20 basins (2% of the study area) prioritized highest in the disrupted order (D) for scenario S_{16}

S ₁₆ order	Basin name (b_i)	State	Basin type	Baseline order (S_1)
1	7080044390	FL	Coastal	10
2	7080044450	FL	Coastal	1
3	7080789240	FL	Inland	4
4	7080696960	SC	Inland	45
5	7080791760	FL	Inland	2
6	7080791840	FL	Inland	20
7	7080684980	SC	Inland	35
8	7080791630	FL	Inland	11
9	7080684850	SC	Inland	73
10	7080691080	SC	Inland	25
11	7080791790	FL	Inland	6
12	7080676370	SC/NC	Inland	36
13	7080667100	SC/NC	Inland	97
14	7080677550	SC/NC	Inland	69
15	7080043160	SC	Coastal	135
16	7080675620	SC	Inland	98
17	7080684690	SC	Inland	96
18	7080690650	SC	Inland	39
19	7080043100	SC	Coastal	147
20	7080675700	SC	Inland	142

Note: The HydroBASINS Level-08 basin name, state, basin type (coastal or inland), and baseline order (S_1) are provided. A reference map of the basin locations is available in Fig. 9(a).

tend to exhibit the lowest order. Thus, this pattern is due to SVI, which is the only variable to prioritize inland basins more than coastal basins.

Table 4 shows the top-20 basins (2%) of prioritization based on the basin ordering of scenario S_{16} . A reference map of the basin locations is shown in Fig. 9(a). This serves as a conservative estimate of which basins should be prioritized because it had the lowest score of disruptiveness. Basins in Florida, South Carolina, and North Carolina are all represented in the top 2% of prioritization. Moreover 20% (4) were coastal basins and 80% (16) were inland. The baseline orders of these basins are within the top 16% of the overall SVI order of the study area. Since these basins ordered in the top 2% of the S_{16} order, it indicates they were also exposed to extreme hydrological conditions due to Hurricane Ian.

Risk as the Disruption of Basin Order

Fig. 8 provides a map of the risk basin order results [calculated using Eq. (3)] for the three scenarios previously examined: S_9 , S_{16} , and S_{19} . It is important to note that if a basin experienced high order in both the baseline map and the disrupted order map, it is reflected as low risk in Fig. 8; the order did not significantly change. The greatest increases in order are found in basins with low social vulnerability but high hydrological exposure. Conversely, the greatest decreases in order are found in basins with high social vulnerability but low hydrological exposure. Thus, this tool is intended to be used in conjunction with the disrupted basin order map (Fig. 7) to identify basins that were disrupted due to exposure to the extreme hydrological conditions.

In Fig. 8(a), the risk map of scenario S_9 had approximately 466 basins (51%) experience an increase in order and thus positive risk (depicted in red). Conversely, 454 basins (49%) decrease in order (depicted in green). Only two basins (less than 1%) have no change in order. This indicates that few basins have both low social vulnerability and low soil moisture conditions.

Similar to the disrupted basin order maps shown in Fig. 7, the risk basin maps are consistent with the path of Hurricane Ian in Figs. 8(b and c). The highest risk basins are found in the Carolinas, while the lowest risk basins are found in Alabama and Georgia. For scenario S_{16} [Fig. 7(b)], 458 basins (~50%) increase in order while

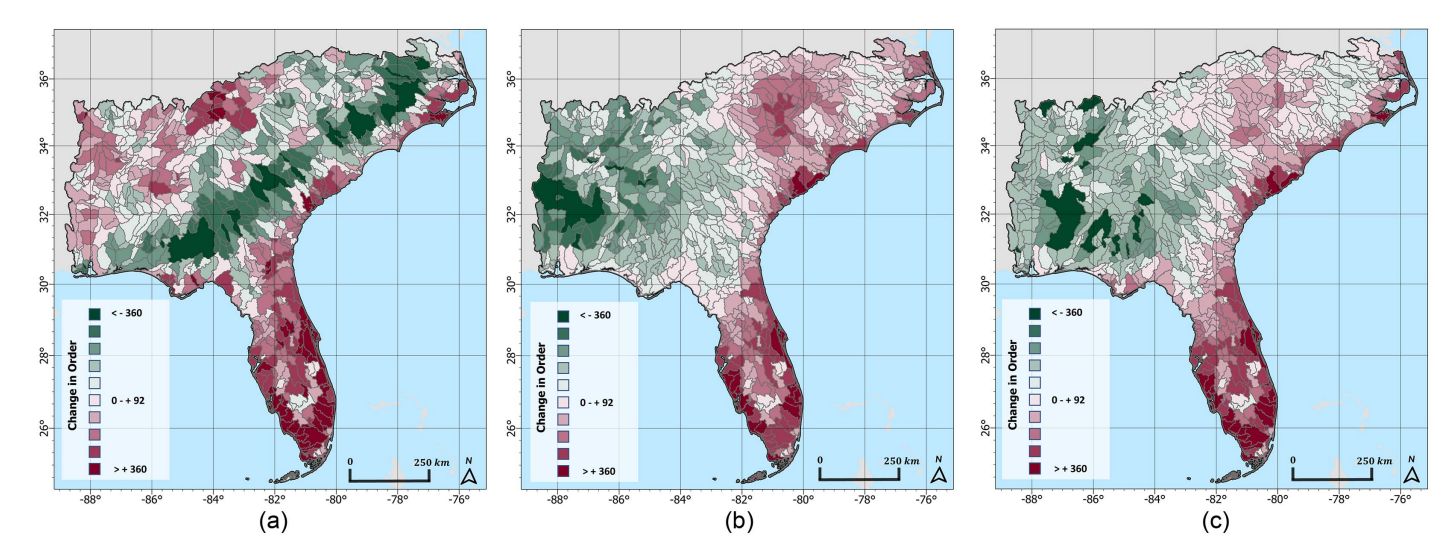


Fig. 8. Spatial plot of the basin risk for the following scenarios: (a) S_9 —SVI and Hurricane Ian 5-day antecedent soil moisture; (b) S_{16} —SVI, Hurricane Ian maximum cumulative precipitation, maximum hourly precipitation, and maximum hourly wind speed; and (c) S_{19} —SVI, Hurricane Ian maximum hourly precipitation, maximum hourly wind speed, and 5-day antecedent soil moisture. Basins that increased in order are depicted in red. Basins that decreased in order are depicted in green.

Table 5. Summary of top 10 basins (1%) with largest increase in priority across scenarios compared to the baseline order (S_1)

	1		*		
Rank of largest increase in priority	Basin name (b_i)	Increase in prioritization (%)	Baseline order (S_1)	Scenario of minimum order (S_n)	Minimum order
1	7080044540	99.35	921	5	5
2	7080044200	98.16	912	3	7
3	7080044210	98.05	913	2	9
4	7080044520	97.94	922	5	19
5	7080044600	97.94	920	5	17
6	7080044460	97.61	901	5	1
7	7080044610	97.51	906	4	7
8	7080044910	96.96	896	2	2
9	7080796400	95.88	893	5	9
10	7080042770	95.01	877	3	1

Note: The rank of largest increase in priority, HydroBASINS Level-08 basin name, increase in prioritization percentage, baseline order (S_1) , scenario of minimum order, and minimum order are provided for each basin. A reference map is shown in Fig. 9(b).

462 (\sim 50%) decrease in order. Few basins had no change in order (two basins, less than 1%). 312 basins (33%) have less than a 10% increase or decrease in order. In scenario S₁₉ [Fig. 8(c)], approximately 422 basins (45%) increase in priority and 496 basins (54%) decrease in priority. Only four basins (less than 1%) have no change in order. However, 343 basins (37%) experience less than 10% increase or decrease in order.

The largest increase in prioritization for the top 10 basins (1%) occurs under scenarios of only one hydrological variable (S_2 , S_3 , S_4 , S_5), with the majority occurring during S_5 (Table 5). The minimum orders under these scenarios are all within the top 2%, indicating these basins had high hydrological exposure. However, the social vulnerability of these basins is within the bottom 95%–100% of the baseline order (i.e., low social vulnerability). The reference map in Fig. 9(b) shows that these basins correspond to areas of protected national parks, national and state preserves, and wildlife management areas and have low populations. Thus, these basins experience large increases in prioritization since their baseline order was low (SVI) but their exposure to hydrological conditions during Hurricane Ian was high.

Similarly, the largest decrease in prioritization for the top 10 basins (1%) occurs under scenarios of only one hydrological variable (S_2 , S_4 , and S_5), with the majority occurring during S_2 (Table 6). The baseline order of all 10 basins is within the top 9% of the baseline order. This indicates these basins are among the most socially vulnerable in the study area. However, the scenario results indicate how these regions had low exposure to hydrological extremes. The reference map shown in Fig. 9(c) shows the basins were located outside of the hurricane path. For the two basins located within the path of Hurricane Ian in the Carolinas, the S_5 scenario was responsible for the highest order, indicating that these basins had very low antecedent soil moisture conditions.

Discussion

Machine Learning for Basin-Level Risk Assessment

One might consider machine learning, a subset of artificial intelligence, in the theory part of this paper. Machine learning has

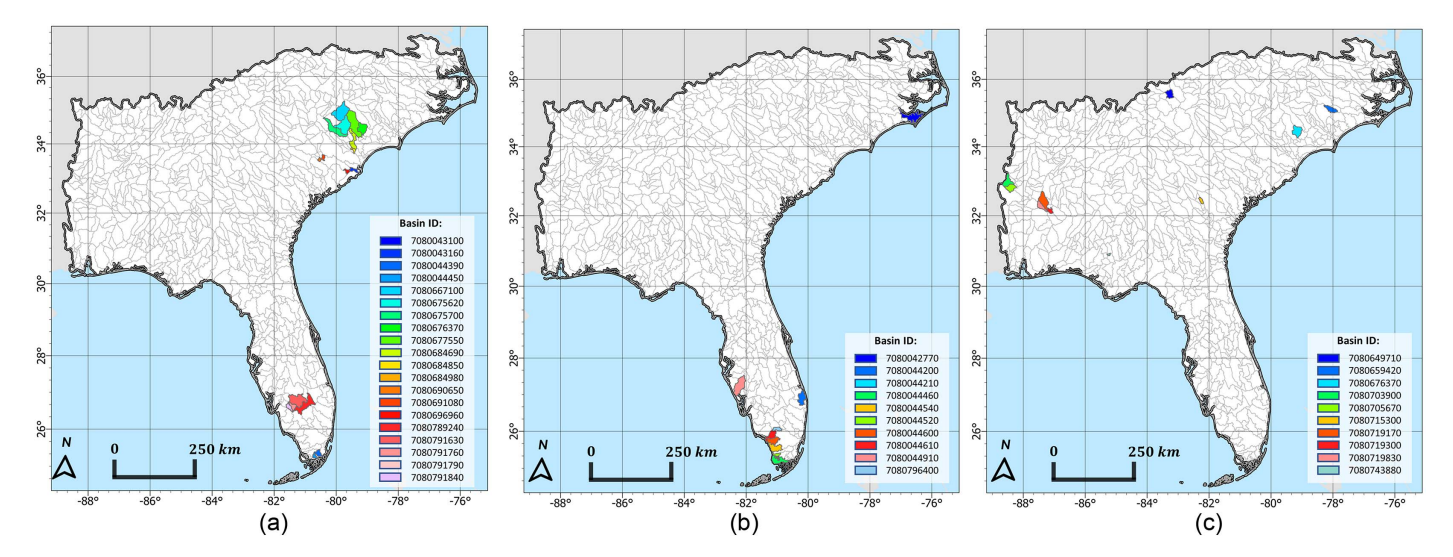


Fig. 9. Reference maps for the following: (a) top 20 basins (2%) with highest prioritization in the disrupted order for scenario S_{16} . A table summary of these basins can be found in Table 4. (b) Top 10 basins (1%) with greatest increase in priority across any scenario compared to the baseline order S_1 . A table summary of these basins can be found in Table 5. (c) Top 10 basins (1%) with greatest decrease in priority across any scenario compared to the baseline order S_1 . A table summary of these basins can be found in Table 6.

Table 6. Summary of top 10 basins (1%) with largest decrease in priority across scenarios compared to the baseline order (S_1)

Rank of largest decrease in priority	Basin name (b_i)	Decrease in prioritization (%)	Baseline order (S_1)	Scenario of maximum order (S_n)	Maximum order
1	7080649710	-97.40	23	4	921
2	7080719300	-95.23	18	2	896
3	7080719830	-94.47	26	2	897
4	7080659420	-93.49	33	5	895
5	7080676370	-93.49	36	5	898
6	7080719170	-93.28	34	2	894
7	7080715300	-93.17	14	5	873
8	7080705670	-91.97	17	2	865
9	7080703900	-91.87	8	2	855
10	7080743880	-90.67	85	5	921

Note: The rank of largest decrease in priority, HydroBASINS Level-08 basin name, decrease in prioritization percentage, baseline order (S_1) , scenario of maximum order, and maximum order are provided for each basin. A reference map is shown in Fig. 9(c).

emerged as a technology to support disaster management given its ability to efficiently process large volumes of data (Reda Taha et al. 2021; Sreelakshmi and Vinod Chandra 2022). This is valuable for supporting disaster predictions, early warnings, response, and recovery efforts (Sreelakshmi and Vinod Chandra 2022).

Theoretically, basin-level risk management could work in partnership with machine learning by using the methodology of this study as a foundational framework. One opportunity for future work is using machine learning to increase the number of factors and complexities of scenarios. However, it is important to ensure any additional data input into the model are derived from reliable, accurate, and spatially complete data (Sreelakshmi and Vinod Chandra 2022). Human supervision may be necessary to avoid unintended algorithm bias, discrimination, and unfairness (Köchling and Wehner 2020).

Validation

Validation of the new approach of this paper has the following considerations. The quantification of risk as a disruption of system

order (following Hassler et al. 2019) is an artifact of an importance model that is grounded in part in the social sciences (social vulnerability) and in part in the physical sciences; the disruption of basin order is not a quantity that is observable either in a storm instance or as a frequency over time. It is useful rather for an integrated comparison of hurricane scenarios and for the allocation of resources to basins in anticipation of hurricane scenarios.

Conclusions

This study developed a methodology to quantify risk as the disruption of basin order by combining social and hydrology factors derived from disparate sources. A swing-weight technique was used to update factor weights of scenarios. This is advantageous for risk analysis using multidisciplinary factors because the relative importance of one variable over another is uncertain. Spatial plots at a subbasin scale of the most and least disruptive scenarios (defined by sum of squares of differences in order) and risk (calculated as the difference in baseline and scenario order) showed geographic

Table 7. Summary of qualitative results of this study including descriptions and figures/tables to reference within this paper

Types of results	Specific results	Comments	Sources
Most disruptive scenarios	S_5 -Hurricane Ian 5-day antecedent soil moisture, S_3 -Hurricane Ian maximum hourly precipitation, S_2 -Hurricane Ian cumulative precipitation	Scenarios of only one contributing variable exhibited the disruptive spatial patterns, relative to the baseline order (S_1) .	Fig. 6, Table 3
Least disruptive scenarios	S_{19} –SVI, Hurricane Ian maximum hourly precipitation, maximum hourly wind speed, and 5-day antecedent soil moisture S_{18} –SVI, Hurricane Ian cumulative precipitation, maximum hourly wind speed, and 5-day antecedent soil moisture	Scenarios of four hydrology and social variables resulted in spatial patterns that were least disruptive to the baseline order (S_1) .	Fig. 6, Table 3
Highest priority basins in disrupted orders	Inland basins of Florida and South Carolina followed by coastal basins of Florida, South Carolina, and North Carolina	Basins of high social vulnerability located within the hurricane path were exposed to the most extreme hydrological conditions and may be prioritized for near-term recovery, response, and future mitigation efforts.	Fig. 7, Table 4, Fig. 9(a)
Lowest priority basins in disrupted orders	Alabama and North Georgia basins	Basins of low social vulnerability located outside the hurricane path had low priority.	Figs. 7 and 8
Greatest increase in basin priority	Coastal basins of Florida	These basins had very high exposure to hydrological conditions during Hurricane Ian but low social vulnerability in the baseline order. They are protected wetlands, nature preserves, parks, and affluent communities with low social vulnerability.	Fig. 8, Table 5, Fig. 9(b)
Greatest decrease in basin priority	Inland basins of Alabama, South Carolina, and North Carolina	These basins had the highest social vulnerability in the baseline order but were located outside the hurricane path, meaning they had low hydrological exposure.	Fig. 8, Table 6, Fig. 9(c)

distribution of basin priority. Stakeholders may use the results as a tool for allocating resources at a basin level to decrease risk and increase resilience.

An application to Hurricane Ian was demonstrated using publicly available data derived from census, models, and Earth observations. A qualitative summary of key findings is provided in Table 7. Scenarios of only hydrology factors identified coastal basins as high-risk areas. However, scenarios of both social vulnerability and hydrology factors identified inland basins as higher risk than coastal basins. Basins of exception to these patterns included protected wildlife management areas within the hurricane path (basins of greatest increase in priority) and basins of high social vulnerability outside the hurricane path (basins of greatest decrease in priority).

It is important to note how the model results can be sensitive to the baseline scenario. For example, medical first responders tasked with selecting locations for temporary medical tents could define the baseline scenario as the SVI subvariable "Aged 65 and Older" (see Appendix II). The differences of system order from the baseline to each of the other scenarios are the focus of interest, and modelers should thus remind the source(s) of the baseline scenario in interpreting the results to stakeholders [see, e.g., (Hassler et al. 2019)].

Future work includes using this study as a framework to explore the capacity of machine learning to increase the number of factors considered and the complexities of scenarios. For the application to major tropical cyclones, future work should explore the relationship of multiple hydrological disasters and social vulnerability over an extended period of time. This would improve understanding of the spatial and temporal patterns of hurricane exposure and social vulnerability in climate-sensitive-hazard regions.

Given the disproportionate impacts of major tropical cyclones and hydrological disasters on socially vulnerable communities, this study provides a tool for risk assessment at the basin level to order basins considering multidisciplinary factors. As demonstrated by the application to Hurricane Ian, results of this work can be used by policymakers and disaster managers to inform future investments designed to decrease the impacts of future major tropical cyclones for vulnerable populations.

Appendix I. Examples of Tropical Cyclone Disaster Challenges Associated with Social Vulnerability

Examples of tropical cyclone disaster challenges associated with social vulnerability during each phase of the disaster cycle include the following:

- Mitigation: Socially vulnerable individuals are less likely to have the financial means to purchase insurance or to live outside of hazard-prone areas (Cutter et al. 2003; Flanagan et al. 2011, 2018; Fothergill and Peek 2004; Yarveysi et al. 2023). Housing structures, such as mobile homes, are typically illequipped to withstand exposure to tropical cyclone conditions (Flanagan et al. 2011; Fothergill and Peek 2004; Yarveysi et al. 2023).
- Preparedness: The socially vulnerable are less likely to have the physical or financial means to evacuate prior to a tropical cyclone (Anand et al. 2023; Flanagan et al. 2011; Meyer et al. 2018). This may stem from a lack of transportation access (i.e., no vehicle, no affordable public transportation alternatives, etc.), an inability to afford evacuation costs (i.e., hotels/temporary lodging, food, fuel, etc.), or a need for increased evacuation assistance (i.e., for the elderly, disabled, and children) (Cutter et al. 2003; Emrich and Cutter 2011; Flanagan et al. 2011).
- Response: Emergency notifications and messaging may not be readily available in languages other than English, making it difficult for racial and ethnic minorities to receive timely

- emergency information if they are not proficient in English (Cutter et al. 2003; Flanagan et al. 2011). If English is not the first language, cultural and language barriers can increase the difficulty of navigating access to postdisaster funding and aid for the socially vulnerable (Cutter et al. 2003).
- Recovery: Communities of high social vulnerability tend to be the slowest to recover following major disasters (Flanagan et al. 2018). Their livelihoods are disproportionately affected by postdisaster damages such as water contamination, loss of sewer systems, power outages, etc. (Cutter et al. 2003).

Appendix II. Summary of Themes and Variables Contributing to Census-Tract Level Social Vulnerability Index Calculation

Themes	Variables
Socioeconomic	1. Below 150% poverty
status	2. Unemployed
	3. Housing cost burden
	4. No high school diploma
	5. No health insurance
Household	1. Aged 65 and older
characteristics	2. Aged 17 and younger
	3. Civilian with a disability
	4. Single-parent households
	5. English language proficiency
Racial and ethnic	1. Hispanic or Latino (of any race)
minority status	Black and African American, not Hispanic or Latino
	 American Indian and Alaska Native, not Hispanic or Latino
	4. Asian, not Hispanic or Latino
	5. Native Hawaiian or other Pacific Islander, not
	Hispanic or Latino
	6. Other races, not Hispanic or Latino
Housing type and	1. Multiunit structures
transportation	2. Mobile homes
	3. Crowding
	4. No vehicle
	5. Group quarters

Source: Data from CDC/ATSDR (2023).

Appendix III. Data Sets Used for Demonstration of the Methodology for Hurricane Ian

Additional details about the data sets used for demonstration of the methodology for Hurricane Ian are given in the subsequent sections.

HydroBASINS

HydroBASINS is a global data set of hierarchical subbasin boundaries at up to 12 scales (Lehner and Grill 2013). This data set is derived from NASA SRTM DEMs at a spatial resolution of approximately 3 arcsec. The nested subbasins are determined by continually delineating two subbasins where two rivers converge, so long as each subbasin maintains a minimum upstream area of at least 100 km² (Lehner and Grill 2013). Additional details of HydroBASINS are available from HydroSHEDS (n.d.).

GPM IMERG

Precipitation data are derived from the Integrated Multi-satellitE Retrievals for Global Precipitation Measurement (GPM IMERG) missions. This satellite constellation of infrared and passive microwave sensors is a joint mission between NASA and the Japan Aerospace and Exploration Agency (JAXA), which provides up to half-hourly precipitation observations at a spatial resolution of 0.1° (Huffman et al. 2020). Previous studies have demonstrated that GPM IMERG adequately detects the spatial variability of major hurricanes, albeit with tendencies to underrepresent precipitation in coastal areas and near the core of hurricanes (Omranian et al. 2018; Pradhan et al. 2022). However, GPM IMERG remains a useful observation for spatial and temporal precipitation estimates during extreme meteorological events because in situ observation systems may suffer instrument failures during hurricanes, as occurred during Hurricane Ian (Bucci et al. 2022). The technical documentation for GPM IMERG is available from NASA (n.d.).

ECMWF ERA5

Wind speed data were obtained from the Copernicus Climate Change Service (C3S) European Centre for Medium-Range Weather Forecast (ECMWF) Reanalysis Version 5 (ERA5). This global reanalysis product, ERA5, is derived from physics-based modeling using both observations and model data as inputs to achieve an atmospheric spatial resolution of approximately 0.25° (Hersbach et al. 2020). Recently, ERA5 has demonstrated an improved representation of tropical cyclones compared to previous ERA versions (Hersbach et al. 2020; Slocum et al. 2022; Zarzycki et al. 2021). The technical documentation of ERA5 is available from ECMWF (n.d.).

SMAP-Derived 1-km Downscaled Surface Soil Moisture Product

The soil moisture active passive (SMAP) derived 1-km downscaled surface soil moisture product is used to calculate the 5-day antecedent near-surface soil moisture (0–5 cm depth below the surface of the Earth) (Lakshmi and Fang 2023). This global data set is derived from the SMAP L-band radiometer and utilizes the moderate resolution imaging spectroradiometer (MODIS) land surface temperature data to downscale soil moisture to a high spatial resolution of 1 km (Fang et al. 2022). This data set has been validated across various biomes and topographies, including within the continental United States, by using networks of in situ soil moisture instruments (Fang et al. 2020, 2022; Pavur and Lakshmi 2023). The data and additional details on the SMAP-derived 1-km downscaled surface soil moisture product are available from NSIDC (n.d.).

Data Availability Statement

All data, models, or code that support the findings of this study are available from the corresponding author upon reasonable request.

Acknowledgments

This paper is based on work supported by the National Science Foundation (NSF) Graduate Research Fellowship Program (GRFP) under Grant No. 182490. Any opinions, findings, conclusions, or recommendations expressed in this work are those of the author(s) and do not necessarily reflect the views of the University of Virginia or the National Science Foundation. The authors are in addition grateful for the support of the Commonwealth Center

for Advanced Logistics Systems, as well as for engagement and feedback from some of the following entities: the United States Army Corps of Engineers (USACE), the United States Agency for International Development (USAID), the Iraq Ministry of Water Resources, attendees of the 2023 European Geophysical Union (EGU) General Assembly, and other local and international collaborators.

Notation

- The following symbols are used in this paper:
 - P1 = cumulative precipitation;
 - P2 = maximum hourly precipitation;
 - R = risk; the difference between the baseline order and scenario order of a given basin;
 - SM = 5-day antecedent soil moisture;
 - *SVI* = basin order using social vulnerability index data; the baseline order;
 - u = u-component of wind in the longitudinal direction 10 m above the surface of the Earth;
 - w = maximum hourly wind speed;
- $X(S_n)$ = normalized score of disruptiveness for a given scenario (S_n) ; the score of disruptiveness for a given scenario $x(S_n)$ minus the minimum score of disruptiveness $(x(S)_{min.})$ divided by the maximum score of disruptiveness $(x(S)_{max.})$ minus the minimum score of disruptiveness $(x(S)_{min.})$; and
- $x(S_n)$ = score of disruptiveness for a given scenario (S_n) ; the sum over the basins of the squared differences of the baseline order and disrupted order.

References

- Anand, H., M. Shafiee-Jood, and N. Alemazkoor. 2023. "Perspicuity of evacuation behavior in communities during hurricanes using largescale mobility patterns and communal characteristics." In Proc., 2023 57th Annual Conf. on Information Sciences and Systems, CISS 2023. New York: IEEE.
- Bakkensen, L. A., C. Fox-Lent, L. K. Read, and I. Linkov. 2017. "Validating resilience and vulnerability indices in the context of natural disasters." *Risk Anal.* 37 (5): 982–1004. https://doi.org/10.1111/risa .12677.
- Bonato, M., B. Sambo, A. Sperotto, J. H. Lambert, I. Linkov, A. Critto, S. Torresan, and A. Marcomini. 2022. "Prioritization of resilience initiatives for climate-related disasters in the metropolitan city of Venice." *Risk Anal.* 42 (5): 931–952. https://doi.org/10.1111/risa.13823.
- Bucci, L., L. Alaka, A. Hagen, S. Delgado, and J. Beven. 2022. National hurricane center tropical cyclone report: Hurricane Ian (AL092022). Washington, DC: American Meteorological Society.
- CDC/ATSDR (Centers for Disease Control and Prevention/Agency for Toxic Substances and Disease Registry/Geospatial Research, Analysis, and Services Program). 2023. "CDC/ATSDR social vulnerability index 2020 database." Accessed May 3, 2024. https://www.atsdr.cdc.gov/placeandhealth/svi/data_documentation_download.html.
- Clark, U., J. E. Ahn, and S. K. Bauer. 2022. "Investigating the impacts of economic factors on recovery to further develop hurricane resilience model for residential homes." J. Risk Uncertainty Eng. Syst. Part A: Civ. Eng. 8 (2): 04022013. https://doi.org/10.1061/ajrua6.0001228.
- Cutter, S. L., B. J. Boruff, and W. L. Shirley. 2003. "Social vulnerability to environmental hazards." Soc. Sci. Q. 84 (2): 242–261. https://doi.org/10 .1111/1540-6237.8402002.
- ECMWF (European Centre for Medium-Range Weather Forecasts). n.d. "ERA5: Data documentation." Accessed May 3, 2024. https://confluence.ecmwf.int/display/CKB/ERA5%3A+data+documentation.

- Emrich, C. T., and S. L. Cutter. 2011. "Social vulnerability to climatesensitive hazards in the Southern United States." Weather Clim. Soc. 3 (3): 193–208. https://doi.org/10.1175/2011WCAS1092.1.
- Fang, B., V. Lakshmi, R. Bindlish, T. J. Jackson, and P. W. Liu. 2020. "Evaluation and validation of a high spatial resolution satellite soil moisture product over the Continental United States." *J. Hydrol.* 588 (Sep): 125043. https://doi.org/10.1016/j.jhydrol.2020.125043.
- Fang, B., V. Lakshmi, M. Cosh, P. W. Liu, R. Bindlish, and T. J. Jackson. 2022. "A global 1-km downscaled SMAP soil moisture product based on thermal inertia theory." *Vadose Zone J.* 21 (2): e20182. https://doi.org/10.1002/vzj2.20182.
- Flanagan, B. E., E. W. Gregory, E. J. Hallisey, J. L. Heitgerd, and B. Lewis. 2011. "A social vulnerability index for disaster management." *J. Homel. Secur. Emerg. Manage.* 8 (1): 0000102202154773551792. https://doi.org/10.2202/1547-7355.1792.
- Flanagan, B. E., E. J. Hallisey, E. Adams, and A. Lavery. 2018. "Measuring community vulnerability to natural and anthropogenic hazards: The centers for disease control and prevention's social vulnerability index." *J. Environ. Health* 80 (10): 34.
- Fothergill, A., and L. A. Peek. 2004. "Poverty and disasters in the United States: A review of recent sociological findings." *Nat. Hazards* 32 (May): 89–110. https://doi.org/10.1023/B:NHAZ.0000026792.76181.d9.
- Hamilton, M. C., J. H. Lambert, and L. J. Valverde. 2015. "Climate and related uncertainties influencing research and development priorities." *J. Risk Uncertainty Eng. Syst. Part A: Civ. Eng.* 1 (2): 04015005. https://doi.org/10.1061/ajrua6.0000814.
- Hassler, M. L., D. J. Andrews, B. C. Ezell, T. L. Polmateer, and J. H. Lambert. 2019. "Multi-perspective scenario-Based preferences in enterprise risk analysis of public safety wireless broadband network." *Reliab. Eng. Syst. Saf.* 197 (May): 106775. https://doi.org/10.1016/j.ress.2019.106775.
- Hersbach, H., et al. 2020. "The ERA5 global reanalysis." *Q. J. R. Meteorol. Soc.* 146 (730): 1999–2049. https://doi.org/10.1002/qj.3803.
- Huffman, G. J., D. T. Bolvin, D. Braithwaite, K. Hsu, R. Joyce, C. Kidd,
 E. J. Nelkin, S. Sorooshian, J. Tan, and P. Xie. 2020. "NASA Global Precipitation Measurement (GPM) Integrated Multi-satellitE Retrievals for GPM (IMERG) Prepared for: Global Precipitation Measurement (GPM) National Aeronautics and Space Administration (NASA)."
 Algorithm Theor. Basis Doc. 4 (26): 30.
- HydroSHEDS. n.d. "HydroBASINS v1.0 data." Accessed May 3, 2024. https://hydrosheds.org/products/hydrobasins.
- Kaplan, S., and B. J. Garrick. 1981. "On the quantitative definition of risk." Risk Anal. 1 (1): 11–27. https://doi.org/10.1111/j.1539-6924.1981 .tb01350.x.
- Karimiziarani, M., and H. Moradkhani. 2023. "Social response and Disaster management: Insights from twitter data Assimilation on Hurricane Ian." *Int. J. Disaster Risk Reduct.* 95 (Sep): 103865. https://doi.org/10.1016/j.ijdrr.2023.103865.
- Karvetski, C. W., J. H. Lambert, and I. Linkov. 2009. "Emergent conditions and multiple criteria analysis in infrastructure prioritization for developing countries." *J. Multi-Criteria Decis. Anal.* 16 (5–6): 125–137. https://doi.org/10.1002/mcda.444.
- Kavvada, A., D. Cripe, and L. Friedl. 2022. Earth observation applications and global policy frameworks. New York: Wiley.
- Köchling, A., and M. C. Wehner. 2020. "Discriminated by an algorithm: A systematic review of discrimination and fairness by algorithmic decision-making in the context of HR recruitment and HR development." *Business Res.* 13 (3): 795–848. https://doi.org/10.1007/s40685-020-00134-w.
- Lakshmi, V., and B. Fang. 2023. "SMAP-Derived 1-km downscaled surface soil moisture product, Version 1." In NASA national snow and ice data center distributed active archive center. Boulder: Univ. of Colorado Boulder. https://doi.org/10.5067/U8QZ2AXE5V7B.
- Lavell, A., C. Rica, M. Oppenheimer, C. Diop, S. Moser, and K. Takeuchi. 2012. "Climate change: New dimensions in disaster risk, exposure, vulnerability, and resilience." In *Managing the risks of extreme events* and disasters to advance climate change adaptation. Cambridge, UK: Cambridge University Press.
- Lehner, B., and G. Grill. 2013. "Global river hydrography and network routing: Baseline data and new approaches to study the world's large

- river systems." *Hydrol. Processes* 27 (15): 2171–2186. https://doi.org/10.1002/hyp.9740.
- Meyer, M. A., B. Mitchell, J. C. Purdum, K. Breen, and R. L. Iles. 2018. "Previous hurricane evacuation decisions and future evacuation intentions among residents of southeast Louisiana." *Int. J. Disaster Risk Reduct.* 31 (Oct): 1231–1244. https://doi.org/10.1016/j.ijdrr.2018.01.003.
- NASA (National Aeronautics and Space Administration). n.d. "Global precipitation measurement IMERG V06 technical documentation." Accessed May 3, 2024. https://www.gpm.nasa.gov/resources/documents/IMERG-V06-Technical-Documentation.
- NOAA (National Oceanic and Atmospheric Administration). 2023. "National centers for environmental information (NCEI) U.S. Billion-Dollar weather and climate disasters (2023)." Accessed May 3, 2024. https://www.ncei.noaa.gov/access/billions/.
- NSIDC (National Snow and Ice Data Center). n.d. "SMAP-Derived 1-km downscaled surface soil moisture product, Version 1." Accessed May 3, 2024. https://nsidc.org/data/nsidc-0779/versions/1.
- Omranian, E., H. O. Sharif, and A. A. Tavakoly. 2018. "How well can global precipitation measurement (GPM) capture hurricanes? Case study: Hurricane Harvey." *Remote Sens.* 10 (7): 1150. https://doi.org/10 .3390/rs10071150.
- Palm, R., and T. Bolsen. 2023. "Perspectives of Southwest Florida homeowners and real estate agents before Hurricane Ian." In *Professional geographer*. London: Routledge.
- Pavur, G., and V. Lakshmi. 2023. "Observing the recent floods and drought in the Lake Victoria Basin using Earth observations and hydrological anomalies." J. Hydrol. Reg. Stud. 46 (Apr): 101347. https://doi.org/10 .1016/j.ejrh.2023.101347.
- Pradhan, R. K., Y. Markonis, M. R. Vargas Godoy, A. Villalba-Pradas, K. M. Andreadis, E. I. Nikolopoulos, S. M. Papalexiou, A. Rahim, F. J. Tapiador, and M. Hanel. 2022. "Review of GPM IMERG performance: A global perspective." *Remote Sens. Environ.* 268 (Jan): 112754. https://doi.org/10.1016/j.rse.2021.112754.
- Reda Taha, M., B. M. Ayyub, K. Soga, S. Daghash, D. Heras Murcia, F. Moreu, and E. Soliman. 2021. "Emerging technologies for resilient

- infrastructure: Conspectus and roadmap." *J. Risk Uncertainty Eng. Syst. Part A: Civ. Eng.* 7 (2): 03121002. https://doi.org/10.1061/AJRUA6 0001134
- Shittu, E., G. Parker, and N. Mock. 2018. "Improving communication resilience for effective disaster relief operations." *Environ. Syst. Decis.* 38 (3): 379–397. https://doi.org/10.1007/s10669-018-9694-5.
- Slocum, C. J., M. Naufal Razin, J. A. Knaff, and J. P. Stow. 2022. "Does ERA5 mark a new era for resolving the tropical cyclone environment?" J. Clim. 35 (21): 7147–7164. https://doi.org/10.1175/JCLI-D-22.
- Smith, A. B. 2023. "U.S. billion-dollar weather and climate disasters, 1980present (NCEI Accession 0209268)." In NOAA national centers for environmental information. Washington, DC: NOAA National Centers for Environmental Information.
- Smith, A. B., and R. W. Katz. 2013. "US billion-dollar weather and climate disasters: Data sources, trends, accuracy and biases." *Nat. Hazards* 67 (2): 387–410. https://doi.org/10.1007/s11069-013-0566-5.
- Sreelakshmi, S., and S. S. Vinod Chandra. 2022. "Machine learning for disaster management: Insights from past research and future implications." In *Proc.*, 2022 Int. Conf. on Computing, Communication, Security and Intelligent Systems (IC3SIS), 1–7. New York: IEEE.
- UNDRR (United Nations Office for Disaster Risk Reduction). 2015.
 Sendai framework for disaster risk reduction 2015-2030. Washington,
 DC: UNDRR.
- Yarveysi, F., A. Alipour, H. Moftakhari, K. Jafarzadegan, and H. Moradkhani. 2023. "Block-level vulnerability assessment reveals disproportionate impacts of natural hazards across the conterminous United States." Nat. Commun. 14 (1): 4222. https://doi.org/10.1038/s41467-023-39853-z.
- You, H., J. H. Lambert, A. F. Clarens, and B. J. McFarlane. 2014. "Quantifying the influence of climate change to priorities for infrastructure projects." *IEEE Trans. Syst. Man. Cybern. Syst.* 44 (2): 133–145. https://doi.org/10.1109/TSMC.2013.2248709.
- Zarzycki, C. M., P. A. Ullrich, and K. A. Reed. 2021. "Metrics for evaluating tropical cyclones in climate data." J. Appl. Meteorol. Climatol. 60 (5): 643–660. https://doi.org/10.1175/JAMC-D-20.